Published Online on 29 June 2016

Proc Indian Natn Sci Acad **82** No. 2 June Spl Issue 2016 pp. 309-319

DOI: 10.16943/ptinsa/2016/48422

Research Paper

Solidification with Buoyancy Induced Convection: Evaluation of Different Mushy Zone Formulations

SUDEEP VERMA[1,2] and ANUPAM DEWAN[2,*]

[1]*Solid State Physics Laboratory, DRDO, Timarpur, Delhi 110 054, India*

[2]*Department of Applied Mechanics, Indian Institute of Technology Delhi, Hauz Khas, New Delhi 110 016, India*

(Received on 25 April 2016; Accepted on 28 April 2016)

A comparative assessment is performed between purely porous formulation of the mushy zone controlled by permeability and the hybrid formulations controlled by both permeability and viscosity of the mushy zone during solidification of a binary alloy. The Darcy's Carman-Kozeny equation is used to model the permeability of the mushy zone in porous formulation for all the models. The first hybrid model employs switching functions to simultaneously control the permeability and viscosity of the mushy zone up to a critical solid fraction and thereafter it switches to a purely permeability controlled porous formulation. The second hybrid model assumes mushy zone to be non-newtonian slurry with the liquid viscosity following a power law up to the critical solid fraction and a permeability controlled porous medium thereafter. A two-dimensional computational domain of aqueous ammonium chloride (NH_4Cl-H_2O) solution employing continuum mixture approach is considered for the analysis. Model with purely porous mushy zone formulation showed higher solutal gradients in the mushy zone resulting in higher solutal buoyancy driven convection in mushy zone along with higher bulk macrosegregation effects in comparison to the hybrid models. Both the hybrid models showed potential of capturing the settled free floating particles and broken dendrites with the non-newtonian slurry hybrid model showing potential of capturing the liquidus irregularities.

Keywords: Phase Change; Mushy Zone; Porosity; Permeability; Columnar Dendritic Morphology, Equiaxed Morphology

Introduction

Modeling of alloy solidification has been a topic of extensive research over the last few decades owing to its significant role in processes, such as, materials processing, metallurgy, crystal growth, welding, purification of metals and casting. Phase change process in the case of alloy solidification is characterized by a mushy zone consisting of both solid and liquid phases formed due to the solidification occurring over a temperature range. Mushy zone encounters significant thermal and solutal gradients on account of release of the latent heat and differences in solute solubility in liquid and solid phases due to thermodynamic constraints. Hence the thermo-solutal convection in the mushy zone significantly affects the overall solute segregation in the solidified domain. Flemings (1974) in his famous book on solidification processing has highlighted these effects in detail. Moreover, the mushy zone has a complicated morphology consisting of interconnected columnar dendrites and free flow floating equiaxed crystals often associated with gradual columnar to equiaxed transition (CET) as the solidification front proceeds, which further adds to the complications in modeling alloy solidification. Another difficulty associated with modeling alloy solidification is the incorporation of microscopic heat and mass transfer effects. These are discussed in the book by Kurz and Fischer (1992).

The above-mentioned facts have led to a significant focus on specialized models to predict the morphological features, heat and mass transfer characteristics of the mushy zone at micro level and

*Author for Correspondence: E-mail: adewan@am.iitd.ac.in; Tel.: 0091-11-26591217

its subsequent coupling with the macroscopic heat and mass transfers requiring large computational resources. Hence, normally this micro-macro coupling is performed at the macro level itself mainly by two approaches. The first approach is based on the classical mixture theory by Bennon and Incropera (1987a, b) and the second approach is based on the volume averaging theory by Beckermann and Viskanta (1993). All the significant advancements thereafter have mainly utilized these two approaches for modeling alloy solidification.

Most of the above-mentioned mushy zone models have been developed using the Darcy's porosity model with the assumption of the columnar-dendritic morphology as described by Brent et al. (1988). However, in the regions of high liquid fraction, mushy zone morphology is predominantly free floating equiaxed and its modeling is relatively complex and less reported. It is usually inadequate to represent the mushy zone having regions of non-stationary solid phase using the Darcy's porosity model. Nikrityuk (2011) has reviewed various hybrid formulations of mushy zones which provide a means to model the non-stationary solid phase. Hybrid models provide a simple approach for modeling the mushy zone as a fluid with increased viscosity below a critical solid fraction and as interdendritic skeleton above the critical solid fraction. Oldenburg and Spera (1992) developed a hybrid model which used switching functions based on the theory of rheology to effectively control both the permeability and viscosity during the solidification. This model handles both the columnar dendritic and equiaxed morphology of the mushy zone. Morvan *et al*. (1999) employed this model to study the effect of latent heat and natural convection on the crystal-melt interface in a Bridgman-Stockbarger furnace. Chakraborty *et al*. (2003) used this model to study the turbulent momentum, heat and species transport during binary alloy solidification. Kund and Dutta (2010) applied this model for modeling the solidification of a liquid aluminium alloy along a cooling slope. Ilegbusi and Mat (1997, 1998) developed a hybrid model which assumed high solid fraction region of the mushy zone as a non-newtonian semi-slurry system following a power law relationship with the rate of deformation and for lower solid fraction it followed the Darcy's porosity model (Brent *et al*. 1988). Later Mat and Ilegbusi (2002) extended this work for predicting macrosegregation in alloy solidification.

It is clear that the development of the solidification modeling is a continuously improving process with employment of different approaches to model specific issues related to solidification of metals and alloys and its proper validation as reviewed by Verma and Dewan (2014).

It is seen that various mushy zone models are available in the literature. However, there is no systematic study performed to access the suitability of these models for specific applications. The objective of the present study is to compare the Darcy's porosity model (Brent et al. 1988) with the hybrid models by Oldenburg and Spera (1992) and Ilegbusi and Mat (1997, 1998) and to delineate the efficacy of each model in capturing the characteristic features of solidification of aqueous NH_4Cl-H_2O system which has been used extensively as an analogous system to experimentally study the solidification characteristics of binary alloy system owing to its transparent nature, solidification characteristics (in terms of mushy zone morphology) similar to alloys and lower melting point. Therefore we have also considered the same system for our study. Models for the above-mentioned three cases were developed using the continuum approach which considers all the three regions, viz., solid, mushy-zone and liquid, as a single-phase thus eliminating the need to explicitly track the interfacial boundary conditions. To account for the discontinuity in the temperature gradient due to the release of the latent heat, the enthalpy formulation (Brent *et al*. 1988) is used for the energy equation in the present study. The detailed model formulation is described in the next section thereafter the results and discussion is presented. Finally, the major findings of the study are summarized in the conclusions.

Model Description

We have considered the solidification of NH_4Cl-H_2O system in a two-dimensional rectangular domain (Fig. 1). The model employs the mixture theory by Bennon and Incropera (1987a) for the micro-macro coupling (temperature solute microsegregation relation) on a fixed grid. We have considered the same geometrical configuration, thermo-physical properties, boundary and initial conditions as those used by Bennon and Incropera (1987b).

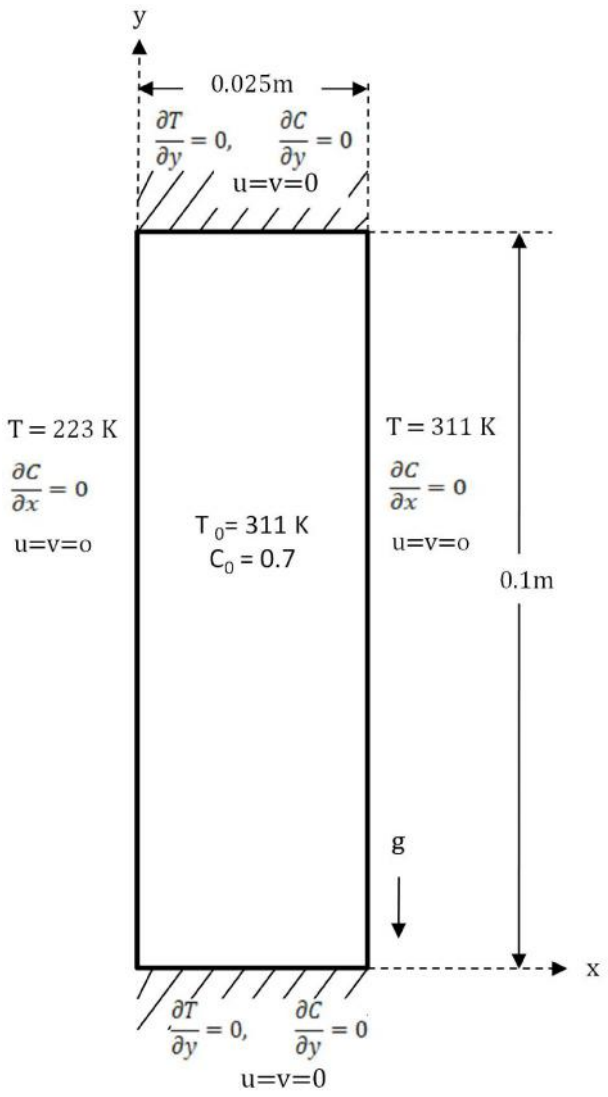

Fig. 1: Schematic of computational domain

Assumptions

(i) The flow is laminar and incompressible.

(ii) Only solid and liquid phases are present and there is no porosity.

(iii) The solid and liquid phases have equal densities and hence shrinkage effects during the solidification are neglected.

(iv) The density is constant except in the buoyancy term of the momentum equation.

(v) The phases are in the local thermodynamic equilibrium and hence equilibrium thermodynamic phase diagram can be used.

(vi) The properties of NH_4Cl-H_2O system are evaluated using the mixture theory.

Governing Equations

The governing equations for 2D planar case are presented in this section.

Equation for conservation of mass equation/ continuity equation

$$\frac{\partial \rho}{\partial t} + \text{div}(\rho \mathbf{u}) = 0 \tag{1}$$

Equation for conservation of x-momentum

$$\frac{\partial(\rho u)}{\partial t} + \text{div}(\rho \mathbf{u} u) = div(\mu_l \text{grad} u) - \frac{\partial p}{\partial x} + Au \tag{2}$$

Equation for conservation of y-momentum

$$\frac{\partial(\rho v)}{\partial t} + \text{div}(\rho \mathbf{u} v) = div(\mu_l \text{grad} v) - \frac{\partial p}{\partial y} + Av + S_b \tag{3}$$

Equation for conservation of energy

$$\frac{\partial(\rho h)}{\partial t} + \text{div}(\rho \mathbf{u} h) = div(\alpha \, \text{grad} h) + S_h \tag{4}$$

Equation for conservation of species

$$\frac{\partial(\rho C)}{\partial t} + \text{div}(\rho \mathbf{u} C) = div(\rho D \text{grad} C) + R \tag{5}$$

According to the mixture theory by Bennon and Incropera (1987a), the mixture density, velocity, enthalpy, species concentration, thermal conductivity and diffusion coefficient are defined as

$$\rho = g_s \rho_s + g_l \rho_l \tag{6}$$

$$\mathbf{u} = f_s \mathbf{u}_s + f_l \mathbf{u}_l \tag{7}$$

$$h = f_s h_s + f_l h_l \tag{8}$$

$$C = f_s C_s + f_l C_l \tag{9}$$

$$K = g_s K_s + g_l K_l \tag{10}$$

$$D = f_l D_l \tag{11}$$

where f_s and f_l, the mass fractions of the solid and liquid phases, respectively, are related to the volume fractions g_s and g_l by the relation

$$\rho f_s = g_s \rho_s, \rho f_l = g_l \rho_l, g_s + g_l = 1 \tag{12}$$

In case both solid and liquid have an equal density, equation (6) is not required.

The sensible enthalpy of the solid and liquid phases are defined as

$$h_s = C_p^s T \text{ and } h_l = C_p^l T + h_f \tag{13}$$

The supplementary relations required for the closure of the above system of equations were obtained from the phase diagram under the assumption of thermodynamic equilibrium. The relation for the temperature solute coupling (micro segregation) described below was obtained using the lever rule:

$$f_s = \frac{1}{1-k_p}\left[\frac{T-T_{liq}}{T-T_m}\right] \tag{14}$$

and the concentrations of solute in solid and liquid are given by

$$C_s = \left[\frac{k_p}{1+ f_s(k_p-1)}\right] C \tag{15}$$

$$C_l = \left[\frac{1}{1+ f_s(k_p-1)}\right] C \tag{16}$$

Model 1: Darcy's Porosity Model (Brent et al., 1988)

This model assumes the morphology of the mushy zone to be columnar dendritic and considers it as a porous medium of a variable permeability (k) given by

$$k = k_0 \frac{f_l^3}{(1-f_l)^2} \tag{17}$$

here k_0 denotes the permeability coefficient and f_l the liquid fraction. The braking effect of a reducing permeability is introduced into the momentum equations via the Darcy's source terms Au and Av defined as

$$Au = -\frac{\mu_l \rho u}{k \rho_l} \text{ and } Av = -\frac{\mu_l \rho v}{k \rho_l} \tag{18}$$

here μ_l denotes the liquid viscosity, ρ and ρ_l the mixture and liquid density and u and v the x and y components of velocity.

Model 2: Hybrid Model by Oldenburg and Spera (1992)

This model employs Eq. (17) for calculating the permeability of the mushy zone for $f_l < 0.5$ and for $f_l > 0.5$, it operates simultaneously on the viscosity (μ_l) and permeability (k) of the mushy zone which are defined as

$$\mu_l = \mu_l^0 \left(\frac{A_\mu}{A_\mu - F f_s}\right)^2 \tag{19}$$

where $A_\mu = 0.4$, $f_s = 1 - f_l$ and μ_l^0 denotes the initial liquid viscosity.

$$k = G k_0 \left[\frac{(1-f_s)^3}{f_s^2}\right] \tag{20}$$

here F and G are the switching functions defined as

$$F = 0.5 - \frac{1}{\pi}\arctan[100(f_s - f_s^{crit})] \tag{21}$$

$$G = \left[0.5 + \frac{1}{\pi}\arctan[100(f_s - f_s^{crit})]\right]^{-4} \tag{22}$$

These switching functions are based on the theory of rheology of suspension and control the Darcy's source term (through the permeability) and the viscosity contributions appropriately. Here the value of f_s^{crit} is taken as 0.5 as used by Chakraborty *et al*. (2003).

Model 3: Hybrid Model by Ilegbusi and Mat (1997)

This model assumes the mushy zone as a non-newtonian semi-slurry system below a critical coherency solid fraction (f_{coh}) for which its viscosity follows a power law given by

$$\mu_l = m\left|\frac{1}{2}(\Delta:\Delta)^{1/2}\right|^{n-1} \quad \text{for } (f_s < f_{coh}) \quad (23)$$

here *m* and *n* denote empirical constants defined as

$$m = \exp(9.783 f_s + 1.435) \text{ and} \quad (24)$$

$$n = 0.105 + 0.41 f_s \quad (25)$$

$$\frac{1}{2}\Delta:\Delta = 2\left(\left(\frac{\partial u}{\partial x}\right)^2 + \left(\frac{\partial v}{\partial y}\right)^2\right) + \left(\frac{\partial u}{\partial y} + \frac{\partial v}{\partial x}\right)^2 \quad (26)$$

where Δ denotes the rate of deformation.

The standard Darcy's porosity model based on the Carman-Kozeny equation (Brent *et al*. 1988) is applied above the coherency point ($f_s > f_{coh}$), where the critical coherency solid fraction (f_{coh}) is defined as the solid fraction at which an interconnected network of dendrites first forms. In the present study the value of for the aqueous NH_4Cl-H_2O system is taken as 0.3 as used by Mat and Ilegbusi (2002). To start the solution initial deformation rate is obtained assuming a constant viscosity (μ_l^0) in the first iteration loop of the first time step. Using the initial deformation rate the viscosity of the mushy zone is varied according to equation (23).

The boundary and initial conditions for the computational domain considered for all the three cases are shown in Fig. 1. The thermo-physical properties of NH_4Cl-H_2O system along with other data used for the numerical simulation are given in Table 1.

Table 1. Thermo-physical properties used for NH_4Cl-H_2O system

Property	Symbol (Unit)	Solid	Liquid
Specific heat	C_p (J $Kg^{-1}K^{-1}$)	1870	3249
Thermal conductivity	K ($Wm^{-1}K^{-1}$)	0.393	0.468
Density	ρ ($Kg\ m^{-3}$)	1078	1078
Diffusion coefficient	D (m^2s^{-1})	—	4.8×10^{-9}
Viscosity	μ_l^0 ($Kg\ m^{-1}s^{-1}$)	—	1.3×10^{-3}
Latent heat of fusion	h_f (JKg^{-1})	3.138×10^5	
Permeability coefficient	k_0 (m^2)	5.56×10^{-11}	
Thermal expansion coefficient	β_T (K^{-1})	3.832×10^{-4}	
Solutal expansion coefficient	β_S	0.257	
Eutectic temperature	T_e (K)	257.75	
Eutectic composition	$C_{l,e}^{\alpha}$	0.803	
NH_4Cl melting point	T_m (K)	633.59	
Equilibrium partition coefficient	k_p	0.3	

Numerical Solution Procedure and Model Validation

The governing equations were discretized and solved using the finite volume method using the commercial CFD software ANSYS FLUENT 15.0. Since the present study involves a comparison of different mushy zone models where non-uniform pressure gradients exist, a staggered grid arrangement was used for capturing the pressure correctly. For the pressure velocity coupling the PISO algorithm was used. We have employed the second order upwind scheme for the discretization of the momentum, energy and species equations. The computational domain was meshed with a 100x100 grid and time step of 0.5s was used. Fig. 2 shows the temperature profiles and velocity magnitudes along the x-direction computed using 50x50, 100x100 and 120x120 grid systems at the location y = 0.05 m (horizontal mid-plane) after 90s. It is observed that the thermal profiles for all grids overlap with each other, however, the velocity profiles do not vary significantly beyond 100x100 grid. Computations at each time step required

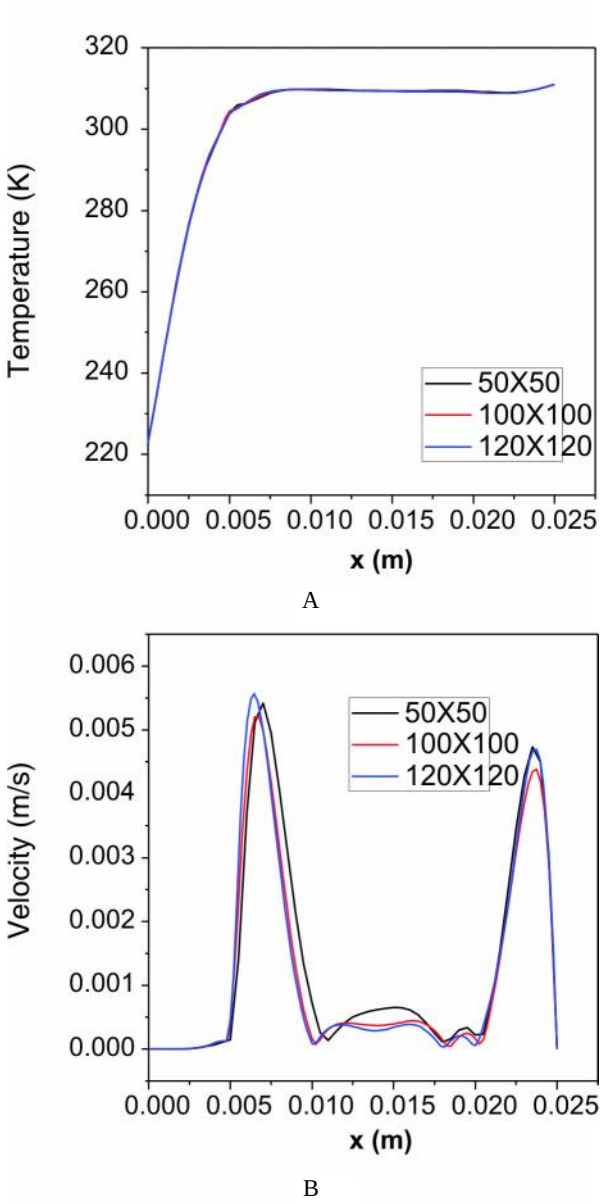

Fig. 2: Results of grid sensitivity for the computational domain (A) temperature (K) and (B) velocity magnitude (m/s) at y = 0.05 m along the x-direction

approximately 200 iterations for convergence.

The developed model was validated with the results of Bennon and Incropera (1987b) using the Darcy's porosity model (Model 1) for the differently heated side walls case. It is observed that the predicted thermal profile [Fig. 3A (1)], velocity stream function profile [Fig. 3B (1)] and liquid species concentration profile [Fig. 3C (1)] agree well with those computed by Bennon and Incropera (1987b) at the same time instant.

Results and Discussion

As shown in Fig. 1, the computational domain is initially kept at a temperature of 311 K. To start the solidification the temperature of the left wall is changed to 223 K. The solidification starts from the left wall and slowly continues in the computational domain. The evolution of the solidification in the computational domain of aqueous NH_4Cl-H_2O system was considered at 90 s, 180 s and 360 s using the above-mentioned three models. Figs. 3-5 show a comparison of the isotherms, streamlines and species concentration at different time intervals.

At t = 90 s isotherms for all the three models [Fig. 3] are curved typically corresponding to strong buoyancy driven convection which generates a typical strong counter clockwise circular loop (generated due to the thermal gradient) in the bulk fluid along with a small clockwise rotating weak loop within the mushy zone (generated due to the solutal gradient). Also the isotherms begin to converge with movement from the bottom to the top. This behaviour is due to an increase in the solute concentration within the mushy zone along the y-direction and it leads to the generation of clockwise interdendritic flow acting against the gravity within the mushy zone. The interaction of this solute rich fluid with the warm bulk fluid moving in the anticlockwise direction driven by the right heated vertical wall locally reduces the growth rate causing a thinning of the mushy region near the top end.

In Model 1 the porous formulation of the mushy zone controls the permeability of the mushy zone completely, i.e., starting from zero solid fraction (liquidus region), the restriction of the bulk flow from entering the mushy region starts. Hence, in comparison to Model 2 (having gradual increase in porosity due to switching functions) and Model 3 (no porous formulation and only viscosity controlled flow at low solid fraction value), comparatively lesser amount of bulk fluid is able to penetrate the mushy zone at the liquidus in Model 1. It is therefore observed that for Model 1, the isotherms diverge near the top wall region as the bulk warm fluid rotating in the anticlockwise direction contributes to a lesser extent in remelting of the dendrites in the top portion of the mushy zone. In Model 2 the permeability is high in comparison to that in Model 1 due to the use of switching functions in its formulation which offers lesser restriction to the entry

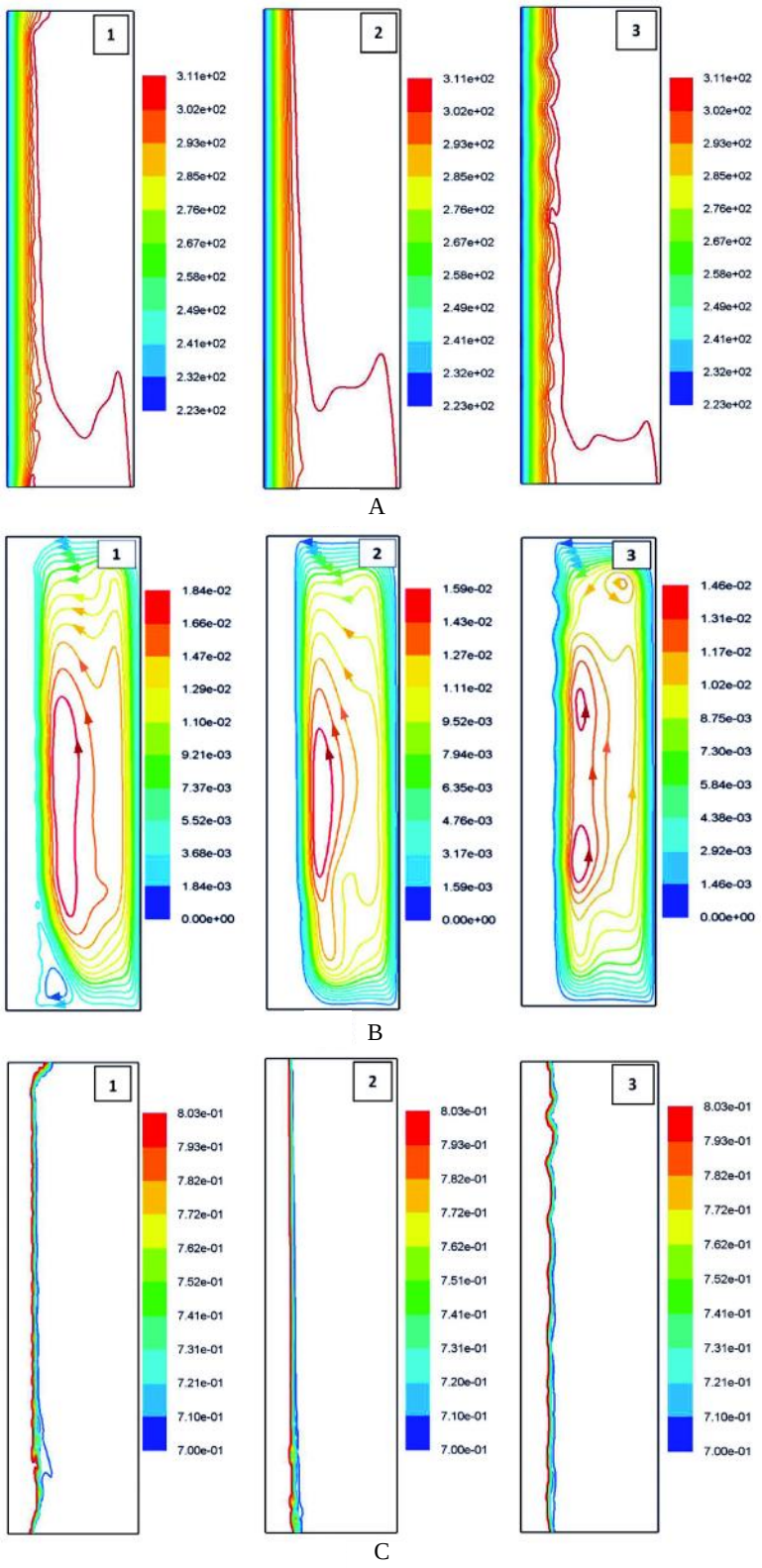

Fig. 3: Comparison of calculated (A) isotherms (K), (B) streamlines (kg/s) and (C) liquid species concentration computed for Model 1 (Darcy's porosity model), Model 2 (Oldenburg and Spera hybrid model), and Model 3 (Ilegbusi and Mat hybrid model) at t = 90 s

of the bulk fluid from entering the mushy region, whereas Model 3 offers no restriction to the bulk fluid from entering the mushy zone near the liquidus region. Hence in these two models thinning of the mushy zone near the top end is observed. It is also observed that the isotherms and the corresponding liquidus shape in the upper half of the domain are comparatively irregular in Model 3. This observation is similar to that by Mat and Ilegbusi (2002) who predicted irregular geometry of the liquidus with this model. This behaviour may be attributed to the capability of the model in capturing the high deformation rate due to the interaction of accumulated solute with high viscosity bulk fluid near the liquidus region.

A comparison of the velocity streamlines at t = 90 s [Fig. 3(B)] shows that the flow field for both Model 1 and Model 2 are undistorted and correspond to strong buoyancy driven flow; however Model 3 shows distortion of the bulk flow field which may be due to the combined effect of the shear forces due to bulk fluid entering the mushy zone and the distortion of flow field due to the liquidus front irregularities. The streamlines corresponding to Model 1 have sharp profiles indicating higher bulk flow strength in Model 1 compared to Model 2 and Model 3. This fact is confirmed by a relatively higher maximum streamfunction value for the flow in Model 1.

A look at the curvature of the liquid species concentration profiles at t = 90 s [Fig. 3(C)] shows high curvature of the iso-composition lines for Model 1 owing to higher solutal gradients due to unperturbed solutal driven convection in the mushy zone. This behaviour is again in line with the above discussion. The counter rotating bulk fluid entering the mushy zone in Model 2 and Model 3 dilutes and homogenises the solute concentration thereby reducing the solutal

gradient resulting in nearly vertical iso-composition lines in the mushy zone for Model 2 and slightly distorted for Model 3 (due to liquidus irregularities as discussed earlier). But this entering bulk fluid is unable to contribute significantly to the advection of the rejected solute into the bulk fluid. This behaviour is evident from the lower macrosegregation effect in Model 2 and Model 3 in comparison to that in Model 1. However at t = 90 s, the bulk macrosegregation is low for all the models as indicated by the values of minimum liquid species concentration in the bulk fluid which is the same as the initial solute concentration of the fluid.

At time t = 180 s and subsequently at t = 360 s (Figs. 4 and 5) the thermal, flow and solutal profiles substantiate the above trends. The mushy zone continued to broaden for Model 1 and similar trend is also noticed for Model 3 at these time instances. Small loops rotating in the clockwise direction appear for Model 2 and Model 3 indicating initiation of the solutal buoyancy. While for Model 3 this loop remained confined to the bottom of the mushy zone, for Model 2 number of smaller loops start emerging along the liquidus line. This indicates that for Model 3 the solutal gradients are confined to the top and bottom of the mushy zone whereas Model 2 showed solutal gradients distributed in small pockets along the length of the mushy zone. This may be attributed to the combined effect of reducing permeability and increasing viscosity while moving from the liquidus towards the solidus region for Model 2. The effect of bulk macrosegregation is seen for Model 1 and Model 3 at t = 360 s with an increase in the minimum liquid species concentration in the bulk fluid. However, the strength of the bulk macrosegregation is less pronounced for Model 3 in comparison to Model 1 due to higher viscosity of the fluid in mushy zone in case of Model 3. It is also seen that Model 2 and Model 3 predict larger mushy region at the bottom of the cavity as shown in Fig. 6. Mat and Ilegbusi (2002) also observed this behaviour with Model 3 and attributed it to the allowance for the motion of free floating

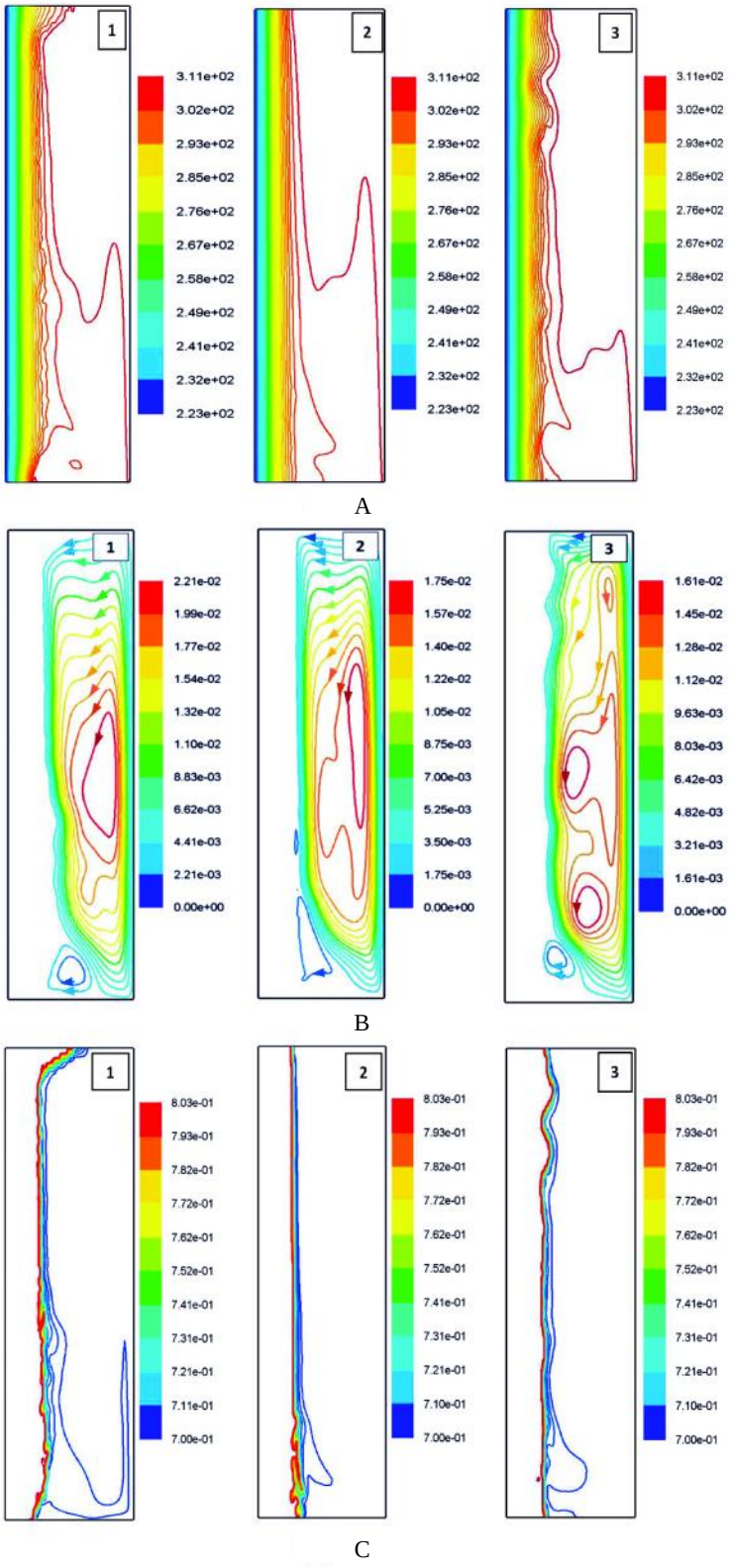

Fig. 4: Comparison of calculated (A) isotherms (K), (B) streamlines (kg/s) and (C) liquid species concentration computed for Model 1 (Darcy's porosity model), Model 2 (Oldenburg and Spera hybrid model), and Model 3 (Ilegbusi and Mat hybrid model) at t = 180 s

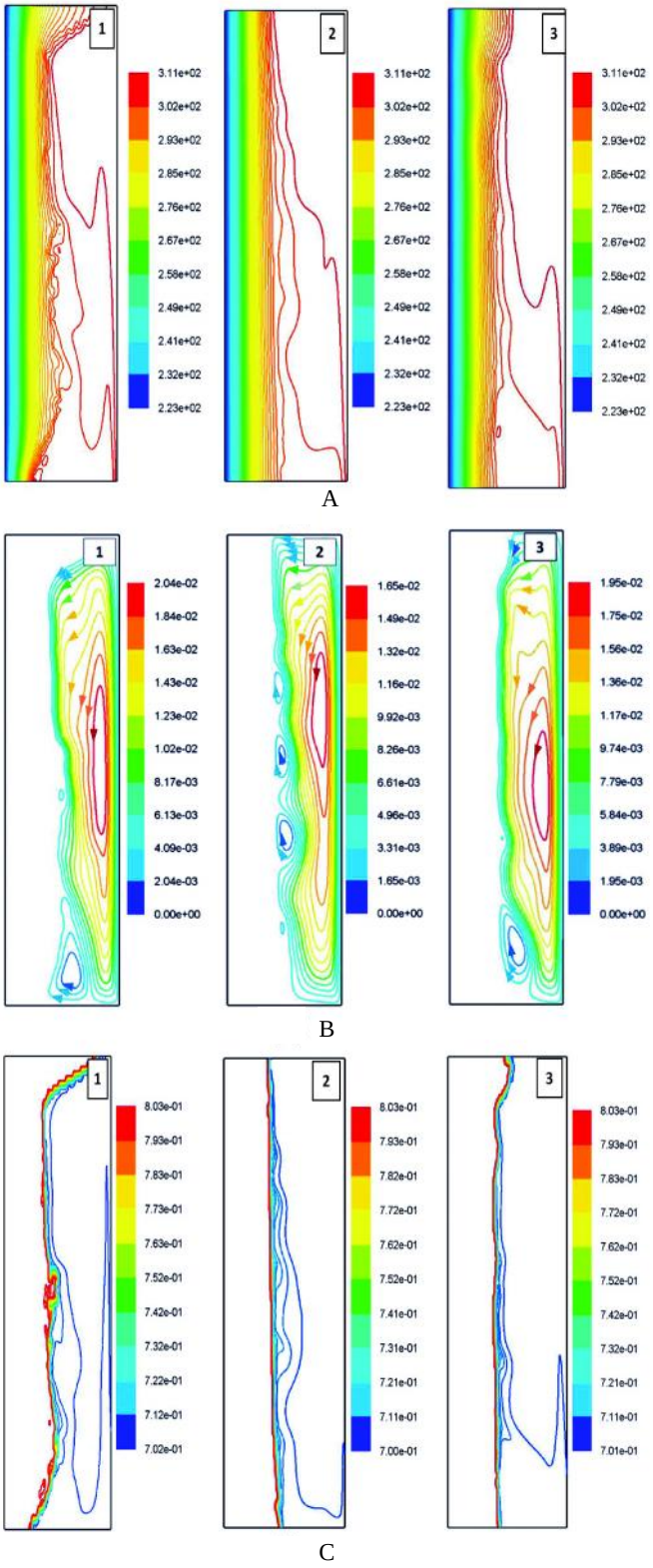

Fig. 5: Comparison of calculated (A) isotherms (K), (B) streamlines (kg/s) and (C) liquid species concentration computed for Model 1 (Darcy's porosity model), Model 2 (Oldenburg and Spera hybrid model), and Model 3 (Ilegbusi and Mat hybrid model) at t = 360 s

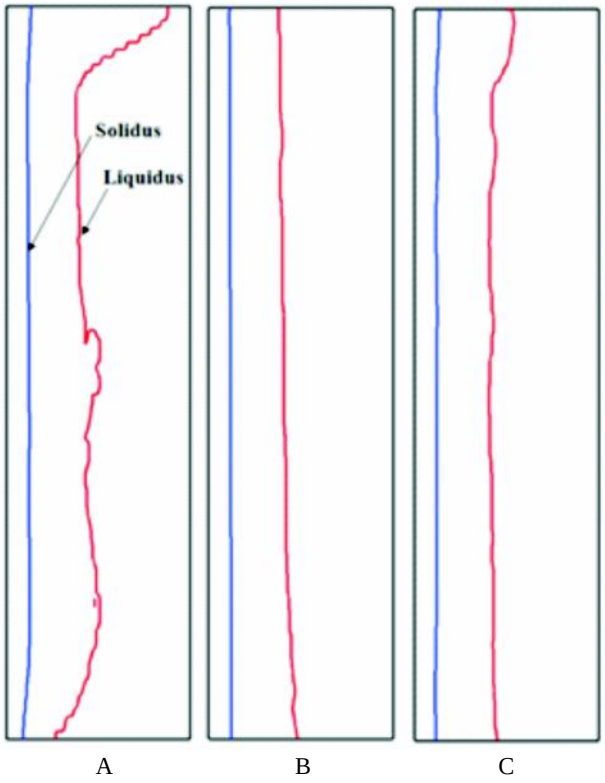

Fig. 6: Comparison of the shape of mushy zone for (a) Model 1 (Darcy's porosity model), (b) Model 2 (Oldenburg and Spera hybrid model), and (c) Model 3 (Ilegbusi and Mat hybrid model) at t = 360 s

particles and broken dendrites in this model. However at the later stages of solidification when the mushy zone increases and effect of decline in permeability within the mushy zone becomes more pronounced, these distinctive characteristics do not magnify further and just continued to follow the set trends.

Conclusion

In the present paper a comparison of two important hybrid models [by Oldenburg and Spera (1992) and Ilegbusi and Mat (1997)] with the generally used Darcy's porosity model is presented for the case of solidification of NH_4Cl-H_2O system in a two-dimensional rectangular domain. The concept of splitting the mushy zone formulation into viscosity and porosity control under the aegis of Darcy's porosity model allows these models to capture both the columnar dendritic and equiaxed morphology of the mushy zone. The distinctive characteristics of the three models are highlighted in terms of the shape of the mushy zone, distribution of solutal gradients within

the mushy zone, interdendritic flow in the mushy zone, irregularity of the liquidus line and the bulk flow field and the bulk macrosegregation effect. The Darcy's porosity model (Model 1) showed higher curvature in isotherms and species concentration profiles along with an early initiation of the solutal buoyancy driven interdendritic flow in the mushy zone along with higher bulk flow strength and bulk macrosegregation. For the hybrid models (Model 2 and Model 3) the isotherms and species distribution profiles were less curved due to the dilution of the solutal gradient region in the mushy zone by the bulk entering fluid. The flow field in the case of Model 3 was irregular in comparison to that in Model 1 and Model 2. Model 3 [hybrid model by Ilegbusi and Mat (1997)] showed characteristics of capturing the liquidus irregularities. Both the hybrid models showed potential of capturing the settled free floating particles and broken dendrites in terms of wider mushy zone at the bottom of the cavity at later stages of solidification.

Notation

Au	x-momentum source term
Av	y-momentum source term
C_s and C_l	species concentration in solid and liquid phases of alloy
C_p^s and C_l^p	specific heat of solid and liquid alloy
D	species diffusion coefficient in alloy
D_l	species diffusion coefficient in liquid alloy
f_s and f_l	mass fractions of the solid and liquid phases
g_s and g_l	volume fractions of the solid and liquid phase
h	sensible enthalpy of the alloy
h_s and h_l	sensible enthalpy of solid and liquid phases of alloy
h_f	latent heat of fusion of alloy
k	permeability
k_0	permeability coefficient
K	thermal conductivity of the alloy
K_s and K_l	thermal conductivities of solid and liquid phases of alloy
p	effective pressure
R	species source term
S_b	buoyancy source term assuming *Boussinesq approximation*
S_h	energy source term
T	temperature
S_{liq}	liquidus temperature corresponding to solute concentration C
T_m	melting point of solvent
$\mathbf{u}(u, v)$	velocity
$\mathbf{u}_l$ and $\mathbf{u}_s$	liquid and solid velocity
α	thermal diffusivity of the alloy
μ_l^0	dynamic viscosity of liquid alloy
ρ	alloy density
ρ_s and ρ_l	solid and liquid density of alloy
Δ	rate of deformation

References

Beckermann C and Viskanta R (1993) Mathematical modeling of transport phenomena during alloy solidification *Appl Mech Rev* **46** 1-27

Bennon W D and Incropera F P (1987a) A continuum model for momentum, heat, mass and species transport in binary solid-liquid phase change system: I. Model formulation *Int J Heat Mass Transfer* **30** 2161-2170

Bennon W D and Incropera F P (1987b) A continuum model for momentum, heat, mass and species transport in binary solid-liquid phase change system: II. Application to solidification in rectangular cavity *Int J Heat Mass Transfer* **30** 2171-2187

Brent A D, Voller V R and Reid K J (1988) Enthalpy-Porosity technique for modeling convection-diffusion phase change: Application to the melting of a pure metal *Numerical Heat Transfer* **13** 297-318

Chakraborty S, Chakraborty N, Kumar P and Dutta P (2003) Studies on turbulent momentum, heat and species transport during binary alloy solidification in a top-cooled rectangular cavity. *Int J Heat Mass Transfer* **46** 1115-1137

Flemings M C (1974) *Solidification processing* McGraw-Hill, New York

Ilegbusi O J and Mat M D (1997) A Hybrid Model of the Mushy Region in Phase-Change Problems *Journal of Materials Processing and Manufacturing Science* **5** 209-224

Ilegbusi O J and Mat M D (1998) Modeling flowability of mushy zone with a hybrid model utilizing coherency solid fraction *Materials Science and Engineering A* **247** 135-141

Kund N K and Dutta P (2010) Numerical simulation of solidification of liquid aluminum alloy flowing on cooling slope *Trans Nonferrous Met Soc China* **20** 898-905

Kurz W and Fisher D J (1992) *Fundamentals of Solidification* Trans Tech Publications Ltd., Switzerland

Mat M D and Ilegbusi O J (2002) Application of a hybrid model of mushy zone to macrosegregation in alloy solidification *Int J Heat Mass Transfer* **45** 279-289

Morvan D Ganaoui M E and Bontoux P (1992) Numerical simulation of a 2-D crystal growth problem in vertical Bridgman-Stockbarger furnace: Latent heat effect and crystal-melt interface morphology *Int J Heat Mass Transfer* **42** 573-579

Nikrityuk P A (2011) *Computational Thermo-Fluid Dynamics*. Wiley-VCH Verlag GmbH & Co., Germany

Oldenburg C T and Spera F J (1992) Hybrid model for solidification and convection. *Numerical Heat Transfer Part B* **21** 217-229

Verma S and Dewan A (2014) Solidification Modeling: Evolution, Benchmarks, Trends in Handling Turbulence, and Future Directions *Metallurgical and Materials Transactions B* **45** 1456-1471.